Available online at www.sciencedirect.com
SCIENCE DIRECT
Applied Catalysis A: General 294 (2005) 197–207
APPLIED CATALYSIS A: GENERAL
www.elsevier.com/locate/apcata

Promoting effect of zinc on the vapor-phase hydrogenation of crotonaldehyde over copper-based catalysts

E.L. Rodrigues [a], A.J. Marchi [b], C.R. Apesteguia [b], J.M.C. Bueno [a,*]

[a] Department of Chemical Engineering, Universidade Federal de São Carlos, Caixa Postal 676, 13565-905 São Carlos (SP), Brazil
[b] Catalysis Science and Engineering Research Group (GICIC), Instituto de Investigaciones en Catálisis y Petroquímica, INCAPE (UNL-CONICET), Santiago del Estero 2654, (3000) Santa Fe, Argentina

Received 7 April 2005; received in revised form 11 July 2005; accepted 16 July 2005

Abstract

The promoting effect of zinc for the vapor-phase hydrogenation of crotonaldehyde was studied on impregnated Cu/SiO_2 and $Cu–ZnO/SiO_2$, and on coprecipitated $Cu–Al_2O_3$ and $Cu_x–Zn_yO_{2y}–ZnAl_2O_4$ catalysts. The reaction was carried out in a tubular reactor at 120 °C and atmospheric pressure. Samples were characterized by temperature-programmed reduction, X-ray diffraction, transmission electronic microscopy, diffuse reflectance FTIR spectroscopy of adsorbed CO, and X-ray photoelectron spectroscopy. Cu/SiO_2 and $Cu–Al_2O_3$ catalysts reduced in hydrogen either at 300 or 500 °C hydrogenated preferentially the C=C bond of crotonaldehyde and gave more than 90% of selectivity to butyraldehyde. In contrast, the initial butyraldehyde selectivity on $Cu–ZnO/SiO_2$ reduced at 500 °C was only about 55%, essentially because the selectivity to crotyl alcohol significantly increased on this zinc-containing sample as compared to Cu/SiO_2. This selectivity enhancement for hydrogenating the C=O bond on $Cu–ZnO/SiO_2$ reduced at 500 °C was explained by considering that the high-temperature hydrogen treatment forms mobile ZnO_x reduced species that strongly interact with Cu^0 crystallites. The resulting $Cu^0–ZnO_x$ species preferentially catalyze the crotyl alcohol formation from crotonaldehyde via a dual-site reaction pathway. A similar explanation was proposed to interpret the observed enhancement of the C=O hydrogenation rate on ternary Cu–Zn–Al catalysts reduced at 500 °C as compared to $Cu–Al_2O_3$. Nevertheless, the $Cu^0–ZnO_x$ species were unstable on stream and the selectivity to crotyl alcohol continuously decreased with reaction time on zinc-containing samples reduced at high temperatures.

Keywords: Crotonaldehyde hydrogenation; Copper-based catalysts; Selective hydrogenation; Zn-promoted catalysts

1. Introduction

Unsaturated alcohols are valuable chemical intermediates for the synthesis of fine chemicals especially used in pharmaceuticals, perfumery and food-processing industry. They can be obtained by selectively hydrogenating the C=O group of α,β-unsaturated aldehydes, but the competitive hydrogenation of the C=C bond is usually faster on noble metals. In general, for short α,β-unsaturated aldehyde molecules, such as acrolein or crotonaldehyde, the C=C group hydrogenation is favored on unpromoted metal catalysts, in terms of both kinetic and thermodynamic considerations [1–3], while for large α,β-unsaturated aldehydes, additional steric constraints imposed by the substituents on the C=C double bond can influence the product selectivity.

The nature of the metal and also the type of crystal face often determine the adsorption mode of the substrate and thereby may control the product selectivity of hydrogenation reactions [4,5]. Thus, to promote the hydrogenation of α,β-unsaturated aldehydes to allyl alcohols, it is required to preferentially adsorb the reactant molecule via the C=O bond and simultaneously deactivate its interaction with the metal surface through the C=C group. Different approaches have been attemped in order to modify the intrinsic adsorption properties of noble metals and increase the selectivity to allyl alcohols. For example, several authors

* Corresponding author. Tel.: +55 16 33518439; fax: +55 16 338466.
E-mail address: jmcb@power.ufscar.br (J.M.C. Bueno).

0926-860X/$ – see front matter © 2005 Elsevier B.V. All rights reserved.
doi:10.1016/j.apcata.2005.07.029

have investigated the influence of the support on metal catalytic properties [1,6–10], while others studied the addition of either a second metal forming bimetallic catalysts or single oxides providing active cationic species [5,11–16]. Promotion by the addition of a second metal has been interpreted in terms of both geometric and electronic effects. The ''dilution'' of the active metal atoms by addition of inert metal atoms (geometric effect) may certainly influence reactant adsorption by diminishing the number of ensembles required for the interaction reactant-active sites. But the second metal may also modify by alloying the electron density of the active metal (electronic effect) and deactivate adsorption of the reactant aldehyde through its C=C double bond. On the other hand, promotion by addition or in situ generation of metal cations has been explained by considering that cationic species act as Lewis acid sites which favor the adsorption of substrate via the C=O group and its consecutive hydrogenation by hydrogen chemisorbed dissociatively on neighbouring metallic sites.

Catalysts based on noble metals, such as platinum [2,11,12,17,18], ruthenium [13,14,19,20], and rhodium [15,16,21,22] have been widely studied for hydrogenation of α,β-unsaturated aldehydes. The use of non-noble metals has also been investigated and the literature reports that cobalt-based catalysts [23–26] show high selectivity to form unsaturated alcohols from α,β-unsaturated aldehydes, in contrast to the case of catalysts based on nickel or copper [27–31]. Attempts to improve the intrinsic catalytic properties of copper and nickel include formation of bimetallic Ni–Cu particles [27] and the interaction between metal and support, as in the case of Cu/Cr_2O_3 [28] and Cu/carbon [29]. Poisoning of copper catalysts by chlorine or sulfur compounds also increases the selectivity to unsaturated alcohol, but at the expense of considerable activity decay [30,31].

In previous studies [32,33], we found that in $Cu/ZnO/SiO_2$ and $Cu/ZnO/Al_2O_3$ catalysts the presence of zinc enhances the copper selectivity towards unsaturated alcohols. Specifically, for the liquid-phase hydrogenation of cinnamaldehyde on Cu^0–$ZnAl_2O_4$ catalysts, we proposed [33] that formation of Cu^0–Zn^{2+} dual-sites provides a new reaction pathway to obtain the cinnamyl alcohol from cinnalmaldehyde. The beneficial effect of Zn was also recently noted by Ammari et al. [34] for the hydrogenation of crotonaldehyde on Pt/ZnO catalysts. These authors proposed that on Pt/ZnO the electronic properties of platinum are modified by both alloying to zinc and ZnO Lewis acidity, thereby favoring the adsorption mode of crotonaldehyde via the C=O bond and subsequent selective formation of crotyl alcohol. In a previous work using Co-based catalysts [26], we observed that addition of ZnO to Co/SiO_2 increases the carbonyl hydrogenation rate of crotonaldehyde. We attributed the superior selectivity of Co–ZnO/SiO_2 catalysts to the formation of surface ZnO_x–Co species that would suppress the activity of metallic Co for hydrogenating the C=C group of crotonaldehyde. However, ZnO_x–Co species, which are formed upon high-temperature catalyst reduction, were not stable on stream and after a relatively long reaction period the selectivity to croyl alcohol on $Co/ZnO/SiO_2$ was similar to that found on ZnO-free catalyst.

In this work, we have extended our previous studies and explored the possibility of improving the intrinsic properties of copper to selectively hydrogenating the carbonyl group of crotonaldehyde. Specifically, we prepared Cu/SiO_2, Cu–ZnO/SiO_2 and ternary Cu–Zn–Al catalysts and compare their activity and selectivity for the gas-phase hydrogenation of crotonaldehyde. The effect of reduction temperature on the formation of Cu^0–ZnO_x species was particularly investigated because it was found that generation of these surface species improve the formation rate of crotyl alcohol. Results will show, in fact, that ternary Cu–Zn–Al catalysts reduced at high temperature exhibit high selectivity to crotyl alcohol because the formation of surface Cu^0–ZnO_x species suppresses the C=C hydrogenation activity and promotes the C=O hydrogenation.

2. Experimental

2.1. Catalyst preparation

Cu/SiO_2 (CuSi) and Cu–ZnO/SiO_2 (CuZnSi) catalyst precursors were prepared by the incipient wetness method, impregnating the support (SiO_2 aerosil-200, Degussa, 200 $m^2\ g^{-1}$) with a methanol solution of Cu and Zn nitrates (Aldrich, 99.999%). The metal salts were dissolved in an appropriate volume of methanol as previously described in detail [25,26]. The precursor was first dried at room temperature and then calcined in synthetic air by heating at 2 °C/min from room temperature to 400 °C and held at this temperature for 2 h.

Ternary Cu–Zn–Al_2O_3 (CuZnAl) catalyst precursors were prepared by coprecipitation in a stirred batch reactor, as described elsewhere [35,36], at pH 7.0 and 60 °C, from a nitrate solution of Cu, Zn and Al, and an aqueous solution of K_2CO_3. The precipitates were aged for 2 h at 60 °C and then filtered and washed with deionized water until the potassium concentration was lower than 0.1% (as K_2O). Then, they were dried at 80 °C overnight, decomposed in N_2 by heating from room temperature to 500 °C at 2 °C/min, and held at this temperature for 6 h. The resulting mixed oxides were reduced in situ by heating in a 60 cm^3/min H_2–N_2 flow (25:75, v/v) from room temperature to reduction final temperature at 10 °C/min, and finally maintaining at final temperature for 2 h.

2.2. Catalyst characterization

The X-ray diffraction (XRD) patterns were collected in an air-tight cell using a Siemens D-5000 diffractometer with Cu Kα radiation (40 kV, 40 mA) and a Ni filter. Copper

crystallite sizes were determined by the Scherrer equation using the average values of (1 1 1) and (2 0 0) line widths. The Warren corrections were used for instrumental line broadening. The lattice constant of Cu was determined by least-squares refinement, from the positions of the Cu peaks.

Temperature programmed reduction (TPR) characterization was performed with a Micromeritics Pulse Chemisorb 2705. The experimental method has previously been described in detail [26].

X-ray photoelectron spectroscopy (XPS) was carried out using a XSAM HS spectrometer from Kratos Analytical. Radiation source was Mg Kα (powered by 15 kV and 15 mA). The pressure in the analysis chamber was 10^{-9} Torr. Samples were flooded with low-energy electrons from a flood gun to avoid charging effect.

The copper metal surface area was determined by reaction with N_2O [37,38]. Sample (about 50 mg) were reduced using the same operative conditions detailed in catalyst testing. After reduction, the flowing N_2/H_2 gas mixture was replaced by a flow of Ar and the reactor temperature was kept at the reduction temperature for 1 h and then cooled to 30 °C. The N_2O chemisorption was then performed at this temperature for 10 min. The amount of superficial Cu^0 was determined by TPR analysis. To calculate the copper metal surface area, it was assumed that equal areas of the (1 0 0), (1 1 0) and (1 1 1) planes were present on the surface, giving a value of 1.35×10^{19} Cu/m^2 [39].

Copper particle sizes were determined by transmission electron microscopy (TEM) in a Philips CM-120 microscope equipped with an EDAX CM-120 elemental analysis probe. Samples were prepared by deposition of an ultrasonic suspension of catalyst particles in isoamylacetate on grids with carbon film.

The infrared spectra for adsorbed CO were collected with a Nicolet Magna 750 infrared spectrometer with diffuse reflectance, Fourier transform and a Spectra Tech cell (DRIFTS). The experimental procedure used has previously been described in detail [25,26].

The deposition of carbonaceous material was characterized by temperature-programmed oxidation (TPO), according to bibliography [40]. Sample (about 20 mg) was heated in a U-tube fused silica, using a 6% O_2/He flow at 60 cm^3/min. The temperature was raised linearly at 10 °C/min to a temperature high enough for complete oxidation of the deposited carbon. The effluent gas, a mixture of CO_2, O_2, H_2O and He, was led into the methanator, which contains 0.5 g of 40 wt.% Ru; Ru/zeolite-13-X. A hydrogen flow of 22 cm^3/min was also injected into the methanator, where CO_2 was transformed to CH_4, and oxygen to H_2O. The rate of oxidation of coke was determined by measuring CH_4 in the effluent by gas cromatography. A FID cromatograph, model 12-800 from Gow-Mac Instrument Co. was used.

2.3. Catalyst testing

Vapor-phase hydrogenation of crotonaldehyde (CROALD) was carried out in a tubular fused-silica microreactor (9 mm i.d.) at 120 °C and atmospheric pressure. Samples were reduced in situ by heating in a H_2–N_2 flow (25:75, v/v) from 25 °C to the desired temperature (between the 300–500 °C range) at 10 °C/min, staying at the final temperature for 2 h. The reactor was then cooled to the reaction temperature. A constant flow of vapor-phase CROALD was established by bubbling the carrier gas mixture, H_2/N_2(1/1, v/v), through a thermostabilized saturator containing liquid CROALD (>99% purity, Aldrich). Reactions were carried out with a crotonaldehyde/H_2/N_2 feed of 1/45/45 at a total flow-rate of 60 cm^3/min and catalysts particle of 0.106–0.150 mm diameter. The feed initially bypass the reactor until a steady-state composition was reached. Reactor effluents were analyzed by on-line gas chromatography, employing a 13 ft 20 M carbowax on a chromosorb-W column.

All gases were purified. N_2 was passed through a Mn-oxytrap and 13X zeolite filter. H_2 was purified by passage through a Pd/Al_2O_3 filter and 13X zeolite filter. The CO line contained carbonyl tramp, filled with quartz, held at a temperature higher than 300 °C.

3. Results and discussion

3.1. Characterization of precursors and calcined precursors

The chemical composition and crystalline structure of catalytic precursors are summarized in Table 1. XRD patterns of coprecipitated CuAl and CuZnAl precursors showed the presence of a single crystalline phase with

Table 1
Chemical composition and crystalline structure of catalytic precursors

Sample	Formulation	Preparation method	XRD analysis	Elemental analysis (wt.%)		
			Hydrated precursor	Cu	Zn	Al
CuSi	Cu/SiO_2	I	Amorphous	14[a]	–	–
CuZnSi	$Cu–ZnO/SiO_2$	I	Amorphus	14[a]	6[b]	–
CuAl	$(CuO)_{0.25}Al_2O_3$	C	Hydrotalcite	13[b]	–	44.3[b]
CuZnAl-1	$(CuO)_{0.4}[ZnAl_2O_4]$	C	Hydrotalcite	11.8[b]	30.4[b]	25.1[b]
CuZnAl-2	$CuOZnO[ZnAl_2O_4]_2$	C	Hydrotalcite	12[b]	37.2[b]	20.5[b]

I = impregnation, C = coprecipitation.
[a] Cu or Zn loading on SiO_2.
[b] wt.% of metal in calcined precursor.

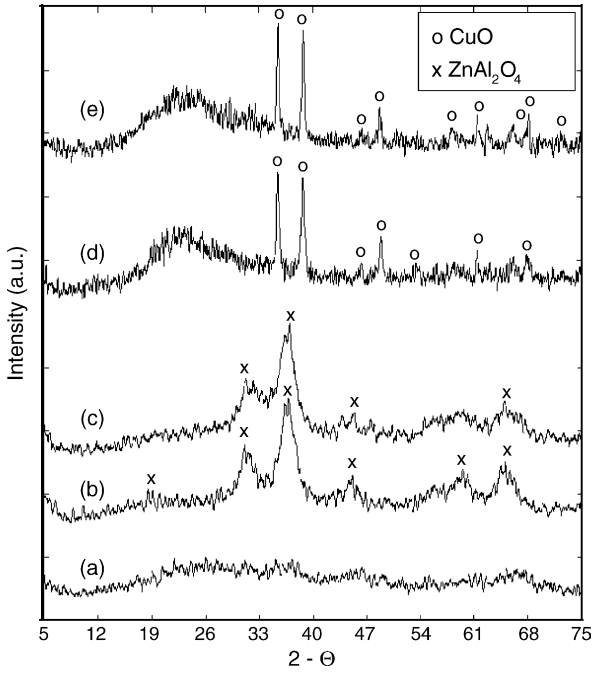

Fig. 1. XRD patterns of calcined precursors: (a) CuAl, (b) CuZnAl-1, (c) CuZnAl-2, (d) CuZnSi and (e) CuSi.

hydrotalcite structure (ASTM 14-191); formation of hydroxides was not detectable. Precursors CuSi and CuZnSi obtained were amorphous.

XRD patterns of calcined precursors are shown in Fig. 1. Calcined CuSi (Cu/SiO_2) and CuZnSi ($CuO–ZnO/SiO_2$) precursors exhibited a single crystalline phase of CuO with tenorite structure (ASTM 5-0661), i.e. ZnO was not detected in $CuO–ZnO/SiO_2$. Crystallographic parameters of CuO phase in $CuO–ZnO/SiO_2$ were $a = 4.742$ Å, $b = 3.4016$ Å and $c = 5.056$ Å, while in CuO/SiO_2 were $a = 4.685$ Å, $b = 3.423$ Å and $c = 5.132$ Å. These results show that the CuO lattice constant was higher in $CuO–ZnO/SiO_2$ than in CuO/SiO_2, and suggest the partial replacement of CuO by ZnO in the tenorite structure of $CuO–ZnO/SiO_2$ sample.

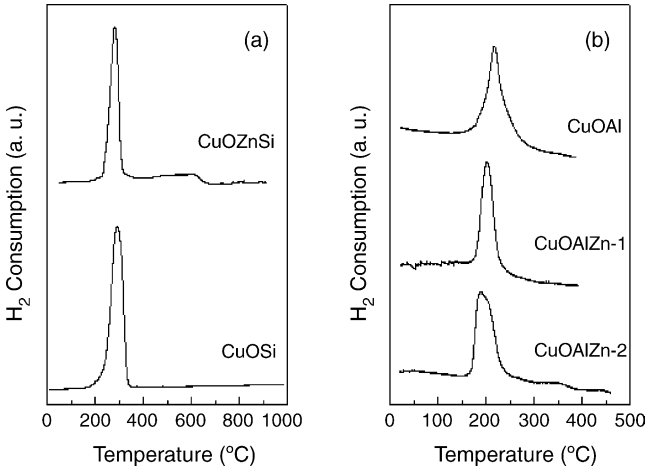

Fig. 2. TPR profiles of calcined precursors.

Calcined CuAl precursor was amorphous. Mixed oxides resulting from calcination of CuZnAl-1 and CuZnAl-2 precursors showed a crystalline $ZnAl_2O_4$ spinel-like phase (ASTM 5-0669 and 10-458). No segregation of CuO or ZnO crystalline phases was detected thereby suggesting that both cations are highly dispersed in the spinel-like phase.

TPR profiles of CuO/SiO_2 and $CuO–ZnO/SiO_2$ (Fig. 2a) showed low-temperature reduction peaks at 293 and 282 °C, respectively, which are assigned to reduction of the CuO phase to Cu^0 [41]. Quantitavely, the H_2 consumption corresponded to total reduction of the CuO phase. $CuO–ZnO/SiO_2$ also exhibited an additional small broad peak between 410 and 680 °C, which probably correspond to the partial reduction of ZnO [42].

TPR profiles of calcined CuAl, CuZnAl-1 and CuZnAl-2 samples (Fig. 2b) showed a single low-temperature reduction peak at 218, 202 and 190 °C, respectively. Similar results for analogous CuZnAl samples were obtained by Marchi et al. [36] who suggested that the low-temperature reduction peaks correspond to reducion of CuO dispersed in a non-stoichiometric zinc aluminate-like phase.

Table 2
XRD, N_2O chemisorption and TEM characterization of the reduced samples

Sample	Reduction temperature (°C)	Condition	Cu^0 particle size (nm)	Cu^0 dispersion[c] (%)	Metallic area[c] (m^2/g Cu)	Cu^0 lattice constant (Å)	Particle composition Zn/(Cu + Zn)[d]
CuSi-LT	300	Fresh	40[a]	4.6	32	3.615	0
CuSi-HT	500	Fresh	38[a]	4.4	31	3.615	0
CuZnSi-LT	300	Fresh	55[a]	9.0	63	3.617	0.017
CuZnSi-HT	500	Fresh	58[a]	3.4	24	3.660	0.208
CuZnSi-HT	500	Used	–	–	–	3.652	0.175
CuAl-LT	300	Fresh	20[b]	17.6	16		
CuZnAl-1-LT	300	Fresh		47.7	335		
CuZnAl-1-HT	480	Fresh	2–7[b]	16.4	115		
CuZnAl-2-LT	300	Fresh		30.0	273		
CuZnAl-2-HT	440	Fresh	2–7[b]	21.6	151		

[a] Obtained from XRD data.
[b] Obtained from TEM data.
[c] Measured by N_2O chemisorption.
[d] Determined from linear correlation with the Cu^0 lattice constant [42].

3.2. Characterization of reduced samples

3.2.1. Characterization by XRD, TEM, N_2O chemisorption, and XPS

CuO/SiO_2 was reduced at 300 °C (CuSi-LT) and 500 °C (CuSi-HT). Characterization by XRD of resulting Cu^0/SiO_2 sample showed that the lattice constant of metallic copper is not modified by the reduction temperature (Table 2). $CuO–ZnO/SiO_2$ was also reduced at 300 °C (CuZnSi-LT) and 500 °C (CuZnSi-HT). The Cu^0 lattice constant in CuZnSi-LT (3.617 Å) was similar to that in CuSi-LT but clearly increased to 3.660 Å in CuZnSi-HT (Table 2). This expansion of the Cu^0 lattice constant suggests that the high-temperature reduction treatment forms reduced ZnO_x species that can migrate and dissolve into the copper particles, as it was proposed by Nakamura et al. [43,44]. Zinc enrichment onto the metallic Cu surface with increasing reduction temperature for a $CuZnO/SiO_2$ catalyst was also observed by Poels and Brands [45] using low-energy ion scattering technique. The electron-diffraction patterns obtained here for CuZnSi-HT sample shows a Cu^0 interplanar distance of $d_{1\,1\,1} = 2.15$ Å (Cu^0 standard, $d_{1\,1\,1} = 2.09$ Å) which is consistent with dissolution of reduced ZnO_x species into the Cu^0 particles. We determined the Zn/(Cu + Zn) ratios into the Cu^0 particle for CuZnSi-LT and CuZnSi-HT samples from linear relation with the lattice constant of Cu^0 obtained by Van Herwijnen and De Jong [42]; results are shown in Table 2.

Table 2 also shows the crystallite size, dispersion and surface area of metallic copper for all the samples. On Cu/SiO_2, copper dispersion did not change with reduction temperature. In contrast, on $Cu–ZnO/SiO_2$ the Cu^0 surface area (as determined by N_2O chemisorption) decreased when the reduction temperature was increased from 300 °C (CuZnSi-LT, 63 m^2/g_{Cu}) to 500 °C (CuZnSi-HT, 24 m^2/g_{Cu}). However, the Cu^0 crystallite size (L_{Cu}) measured by XRD peak broadening was similar on $Cu–ZnO/SiO_2$ reduced at 300 and 500 °C, about 55 nm (Table 2). These results are consistent with the postulation that the high-temperature reduction forms mobile ZnO_x species that partially cover the metallic copper phase. Similarly to $Cu–ZnO/SiO_2$ sample, a strong decrease in the accessible Cu^0 surface area with increasing reduction temperature was observed on ternary CuZnAl samples (Table 2).

Table 3
Metallic surface area of CuZnSi- and CuZnAl-samples after various treatments

Sample	Treatment	Metallic area (m^2/g Cu)
CuZnSi-LT	(I) Reduction at 300 °C for 2 h	63
CuZnSi-HT	(II) Reduction at 500 °C for 2 h	24
CuZnSi-HT	(III) Reduction at 500 °C for 2 h, treatment with N_2O at 30 °C for 12 h, and reactivation at 500 °C for 2 h	45
CuZnSi-HT	(IV) Reduction at 500 °C for 2 h, treatment with N_2O at 30 °C for 12 h, and reactivation at 500 °C for 2 h	21
CuZnAl-2-LT	(I) Reduction at 300 °C for 2 h	273
CuZnAl-2-HT	(II) Reduction at 440 °C for 2 h	151
CuZnAl-2-HT	(III) Reduction at 440 °C for 2 h, treatment with N_2O at 30 °C for 12 h, and reactivation at 300 °C for 2 h	179

In order to obtain more insight on the effect of reduction treatment on the interaction between Cu and Zn, we performed additional experiments using CuZnSi and CuZnAl-2 samples that are described in Table 3. As mentioned previously, on CuZnSi sample the accessible Cu^0 surface area decreased from 63 to 24 m^2/g_{Cu} by increasing the reduction temperature from 300 to 500 °C (Table 3, treatments I and II). When the sample was reduced at 500 °C, but then treated with N_2O at 30 °C for 12 h and finally reduced at 300 °C (treatment III), S_{Cu} was 45 m^2/g. A similar treatment, but performing the final reduction at 500 °C (treatment IV), decreased S_{Cu} to 21 m^2/g_{Cu}, a similar value than that obtained after treatment II. These results suggest that on sample $Cu–ZnO/SiO_2$ reduced at 500 °C the exposure to N_2O partially decomposes $Cu–ZnO_x$ species forming ZnO and liberating metallic Cu that is detected after reduction at 300 °C (treatment III). If the final reduction is performed at 500 °C, then the $Cu–ZnO_x$ species are formed again and the accessible Cu^0 surface area diminishes (treatment IV).

Table 3 also shows that on CuZnAl-2 sample S_{Cu} diminished from 273 to 151 m^2/g_{Cu} by increasing the reduction temperature from 300 to 440 °C (treatments I and II). When CuZnAl-2 reduced at 440 °C was treated with N_2O at 30 °C for 12 h and then reduced at 300 °C, the Cu^0 surface area increased to 179 m^2/g_{Cu} (treatment III). Qualitatively, the S_{Cu} changes were similar on CuZnSi and CuZnAl-2 samples: the high-temperature reduction diminishes S_{Cu} but a consecutive treatment with N_2O partially restores it. However, the S_{Cu} variations were quantitatively more important on CuZnSi than on CuZnAl-2, probably because the reduction temperature and Cu^0 crystallite size were higher for CuZnSi sample.

Finally, the effect of reduction temperature on CuZnSi and CuZnAl samples was studied by XPS technique; results are given in Table 4. A significant drop of the surface Cu/Zn ratio is observed for all the samples following the high-temperature reduction treatment. This result gives additional support to the assumption that hydrogen treatment at high temperature forms mobile ZnO_x species from ZnO that partially cover the surface Cu^0 area.

3.2.2. Characterization by DRIFT

As it is well known, CO is weakly adsorbed on Cu^0 and Cu^{2+} at room temperature [46]. Consistently, we obtained low-intensity infrared absorption peaks of CO chemisorbed on reduced Cu/SiO_2, $Cu–ZnO/SiO_2$ and CuZnAl catalysts. Instead, the heat of adsorption for CO on Cu^+ is considerably strong at room temperature [46]. The different interaction strengths of CO with Cu^0, Cu^+ and Cu^{2+} can lead to

Table 4
XPS parameters of CuZnSi- and CuZnAl-samples

Sample	Reduction temperature (°C)	Cu/Zn		Cu/Si		Cu/Al		Zn/Si		Zn/Al	
		Bulk	Surface	Bulk	Surface	Bulk	Surface	Bulk	Surface	Bulk	Surface
CuZnSi-LT	300	2.29	0.30	–	0.021	–	–	–	0.069	–	–
CuZnSi-HT	500	2.47	0.21	–	0.015	–	–	–	0.027	–	–
CuZnAl-1-LT	300	0.41	0.23	–	–	0.20	0.072	–	–	0.49	0.31
CuZnAl-1-HT	480	0.41	0.16	–	–	–	0.049	–	–	–	0.30
CuZnAl-2-LT	300	0.033	0.25	–	–	0.25	0.077	–	–	0.75	0.31
CuZnAl-2-HT	440	0.33	0.17	–	–	–	0.052	–	–	–	0.30

erroneous conclusions if the corresponding relative peak intensities, obtained at room temperature, are compared. Taking this into account, only the spectra of CO adsorbed on copper re-oxidized samples are shown in this work.

DRIFT spectra of CO adsorbed on CuSi-LT sample exhibited three bands at 2170, 2122 and 2100 cm^{-1}, which can be assigned to CO linearly adsorbed on Cu^{2+}, Cu^{+} and polycrystalline Cu^{0} sites, respectively [46]. The CO adsorption on CuSi-HT gave rise to IR bands centered at similar positions to those observed for CO on CuSi-LT. On the other hand, the CO adsorption on CuZnSi-LT sample showed bands at 2125 and 2106 cm^{-1}, that were hardly detected on CuZnSi-HT. The CO absorption spectrum on CuZnAl-1-LT was similar to that obtained on CuZnSi-LT sample. In contrast, the CO absorption spectrum on CuZnAl-2-LT showed only one band centered at 2105 cm^{-1}. On increasing the reduction temperature from 300 to 440 °C, the adsorption of CO on both CuZnAl samples was strongly suppressed and no CO-IR absorption bands were detected.

After N_2O treatment of the CuSi-LT sample and adsorption of CO, just one symmetric peak at 2122 cm^{-1} was observed, which may be assigned to CO adsorbed on a Cu_2O film [46,47], formed by surface oxidation with N_2O (Fig. 3a). This peak was almost completely removed by heating up to 80 °C (Fig. 4), in agreement with the fact that CO is adsorbed on Cu^{+} but not on Cu^{0}.

After treatment with N_2O and adsorption of CO, the CuZnSi-LT sample showed an asymmetric band at 2122 cm^{-1} with a shoulder at 2114 cm^{-1} (Fig. 3b). This asymmetric band can be convoluted into two symmetric bands with maxima at 2115 and 2124 cm^{-1}, which can be again attributed to CO adsorbed on two different type of Cu^{+} sites. The thermal stability of the CO adsorbed on CuZnSi-LT was sligthly higher than on CuSi-LT (Fig. 4).

The previous results are suggesting that there are some surface structure differences between CuSi and CuZnSi samples. First of all, a different type of copper sites are present on CuZnSi-LT surface that are not detected on CuSi-LT surface. It is likely that ZnO presence is the responsible for generation of this new type of copper sites that gives an infrared peak at lower frequency on the re-oxidized sample. Second, interaction of CO with this new type of Cu^{+} sites is

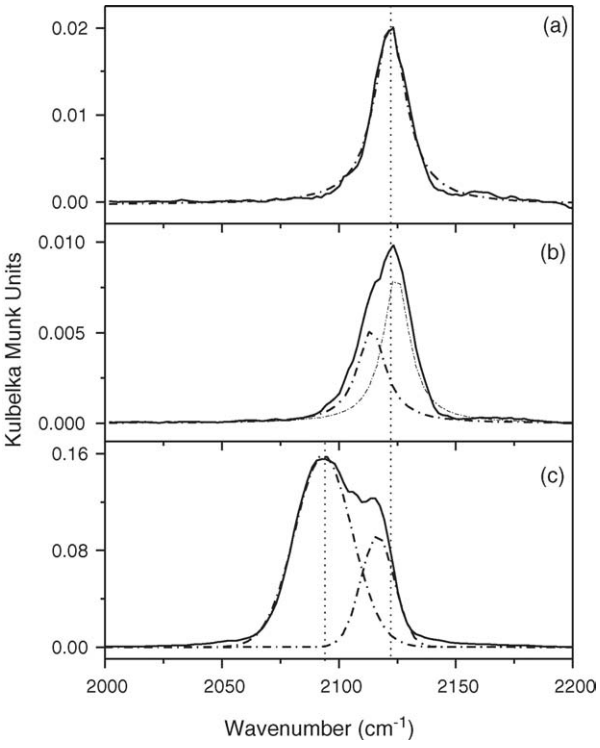

Fig. 3. DRIFT spectra of CO adsorbed at room temperature on (a) CuSi-LT, (b) CuZnSi-LT and (c) CuZnAl-2-LT samples after re-oxidation with N_2O at 30 °C.

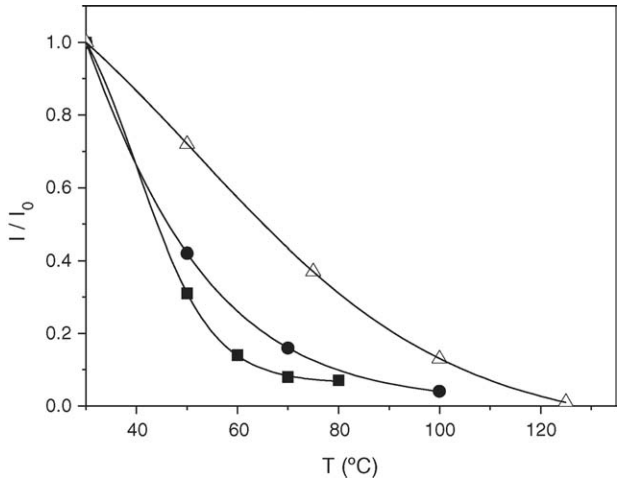

Fig. 4. Relative intensities (I/I_0) of the infrared absorption bands of linear chemisorbed CO on Cu^{+} as a function of desorption temperature for (■) CuSi-LT, (●) CuZnSi-LT and (△) CuZnAl-2-LT. I_0, total intensity of the corresponding infrared bands at 30 °C.

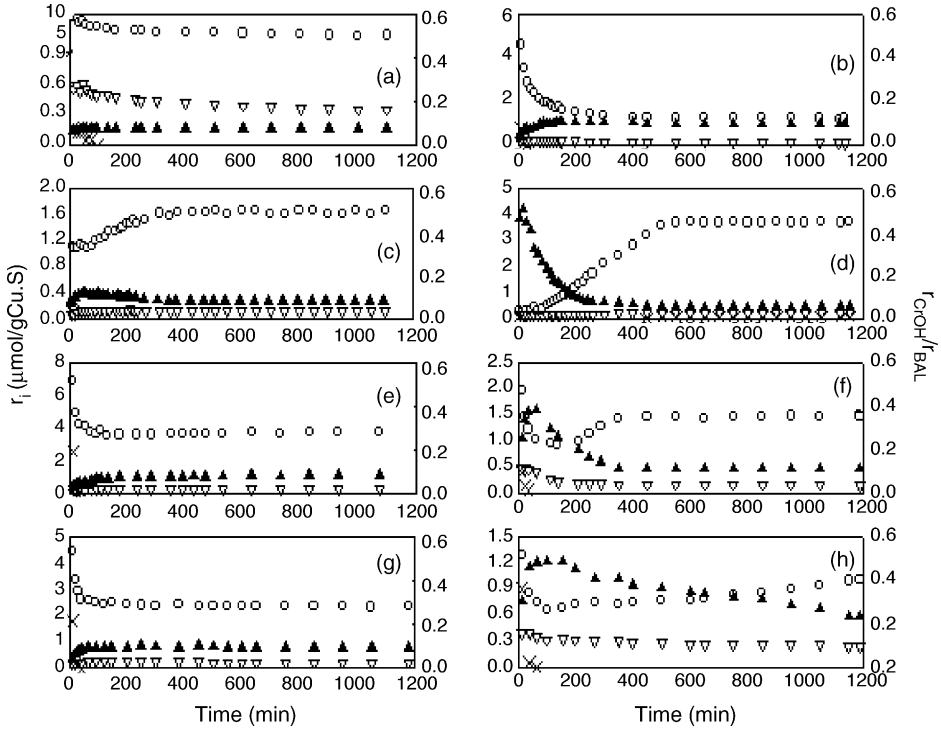

Fig. 5. Product formation rates: (a) CuSi-LT, (b) CuAl-LT, (c) CuZnSi-LT, (d) CuZnSi-HT, (e) CuZnAl-1-LT, (f) CuZnAl-1-HT, (g) CuZnAl-2-LT, (h) CuZnAl-2-HT. Products shown by: (○) BAL, (▽) CrOH, (×) BOL and (▲) r_{CrOH}/r_{BAL}.

stronger than that with the site giving an infrared band of adsorbed CO at higher frequency.

After treatment with N_2O of CuZnAl-2-LT sample and adsorption of CO, a very broad band with a maximum at 2093 cm^{-1} and a shoulder at 2115 cm^{-1} was detected (Fig. 3c). No band at 2122–2124 cm^{-1} was observed for this case. The broad asymmetric band can be fit with two symmetric bands with maxima at 2093 and 2116 cm^{-1}. Although the frequency of the band at 2093 cm^{-1} seems to be low for a copper oxidized species, the high thermal stability observed is characteristic of Cu^+ sites (Fig. 4). Even more, the thermal stability of adsorbed CO on oxidized CuZnAl-2-LT was the highest for this sample series (Fig. 4). Again, the shift of the bands to lower frequency and the former highest stability can be associated with generation of new type of copper sites due to Cu–ZnO interaction, which is favored by the high dispersion of copper in the spinel-like matrix.

The position of the peaks and the different thermal stability for the chemisorbed CO species indicates important differences of metal surface structure for CuZnAl sample respect to CuZnSi and CuSi samples. Furthermore, the highest intensity of infrared bands of adsorbed CO for re-oxidized CuZnAl-2-LT sample is in agreement with the highest dispersion of the reduced CuZnAl sample determined by other methods (Fig. 3 and Table 2).

3.3. Catalytic results

3.3.1. Initial catalyst activity and selectivity

The products formed during crotonaldehyde hydrogenation were essentially butyraldehyde (BAL), crotyl alcohol (CrOH) and butanol (BOL). In Fig. 5, we have plotted both the product formation rates and the r_{CrOH}/r_{BAL} ratio as a function of time on stream. Because all the samples

Table 5
Product formation rates, r_i (μmol g Cu^{-1} s^{-1})

Sample	r^0_{CrOH}	r^0_{BAL}	r^0_{BOL}	r^0_{CrOH}/r^0_{BAL}	r^1_{CrOH}	r^1_{BAL}	r^1_{CrOH}/r^1_{BAL}	r^2_{CrOH}	r^2_{BAL}	r^2_{CrOH}/r^2_{BAL}
CuSi-LT	0.61	9.58	0.167	0.064	0.48	6.33	0.076	0.33	4.39	0.075
CuSi-HT	0.53	9.48	0.183	0.056	0.53	6.15	0.086	0.36	4.56	0.079
CuZnSi-LT	0.069	1.10	0.111	0.063	0.113	1.18	0.096	0.119	1.67	0.071
CuZnSi-HT	0.170	0.300	0.056	0.57	0.131	0.59	0.222	0.226	3.67	0.062
CuAl-LT	0.236	4.86	0.917	0.049	0.182	1.73	0.105	0.111	1.17	0.095
CuAlZn-1-LT	0.278	7.50	2.67	0.037	0.236	3.63	0.065	0.314	3.78	0.083
CuAlZn-1-HT	0.583	2.14	0.444	0.270	0.442	1.00	0.442	0.167	1.44	0.116
CuAlZn-2-LT	0.208	4.86	1.94	0.043	0.241	2.50	0.096	0.233	2.36	0.099
CuAlZn-2-HT	0.472	1.44	1.00	0.328	0.312	0.72	0.433	0.242	1.02	0.237

Note: r^0_i, initial reaction rates; r^1_i, reaction rates obtained at the end of the deactivation period; r^2_i, steady-state reaction rates.

deactivated during the catalytic tests, we also show in Table 5; the values of product formation rates determined at $t = 0$. Copper supported on silica and reduced at 300 °C (CuSi-LT), formed mainly butyraldehyde (Fig. 5a) giving a r^0_{CrOH}/r^0_{CrOH} ratio of 0.064 (Table 5). Initial turnover formation rates (TOF^0, h^{-1}) of butyraldehyde and crotyl alcohol on Cu/SiO_2 reduced at 500 °C (CuSi-HT, $TOF^0_{BAL} = 46.6\,h^{-1}$, $TOF^0_{CrOH} = 2.9\,h^{-1}$) were similar to those determined for CuSi-LT reduced at 300 °C ($TOF^0_{BAL} = 49.5\,h^{-1}$, $TOF^0_{CrOH} = 3.2\,h^{-1}$) showing that the reduction temperature did not modify significantly crotonaldehyde conversion reactions. The product selectivity of binary coprecipitated CuAl sample reduced at 300 °C (Fig. 5b, CuAl-LT) was also similar to that determined for sample CuSi-LT, showing a r^0_{CrOH}/r^0_{BAL} ratio of 0.049 (Table 5).

Initial crotonaldehyde conversion rate on Cu–ZnO/SiO_2 reduced at 300 °C (CuZnSi-LT, Fig. 5c) was significantly lower than on CuSi-LT (Table 5); for example, the BAL turnover formation rate decreased from 49.5 h^{-1} (CuSi-LT) to 2.8 h^{-1} (CuZnSi-LT). However, the r^0_{CrOH}/r^0_{BAL} ratio was similar on both catalysts, about 0.06. The low crotonaldehyde conversion rate observed on CuZnSi-LT may be explained by considering that the presence of Zn on the Cu surface hampers the dissociative hydrogen adsorption and, consequently, decreases the crotonaldehyde hydrogenation rate. But, we cannot exclude the possibility that ZnO preferentially interacts with highly uncoordinated Cu sites on polycrystalline Cu–ZnO/SiO_2 sample thereby suppressing more active hydrogenation sites, as it was proposed to occur on Ni/Al_2O_3 promoted with K [48].

The r^0_{CrOH}/r^0_{BAL} ratio on Cu–ZnO/SiO_2 reduced at 500 °C (CuZnSi-HT, Fig. 5d) was 0.57, significantly higher than that determined on CuZnSi-LT (0.063). This selectivity increase to the formation of crotyl alcohol was caused by the activity enhancement for hydrogenating the C=O bond (TOF^0_{CrOH} increased from 0.17 h^{-1} on CuZnSi-LT to 0.66 h^{-1} on CuZnSi-HT), but also by the diminution of butyraldehyde formation rate (Table 5). Similar effect of Zn promotion on selectivity to CrOH was observed in a previous paper on CoZnO/SiO_2 catalysts [26]. Taking into account that copper-free ZnSi catalysts were inactive for crotonaldehyde hydrogenation at 120 °C, and our TEM and XPS results, it is reasonable to suppose that promotion of the C=O hydrogenation rate on CuZnSi-HT is due to a partial coverage of the Cu surface by ZnO_x species that takes place because the high temperature hydrogen treatment increases the mobility of ZnO_x species. Formation of Cu–ZnO_x species may provide a new reaction pathway for selectively hydrogenating crotonaldehyde to crotyl alcohol. Cationic Zn sites probably adsorb crotonaldehyde via the C=O group thereby favoring its activation. Metallic copper adsorbs H_2 dissociatively and furnishes by spillover the activated atomic hydrogen necessary to hydrogenate the C=O group in crotonaldehyde molecules. A close interaction between Cu^0 and Zn^{2+} active sites appears therefore crucial to efficiently catalyze the crotyl alcohol formation from crotonaldehyde via a dual-site reaction pathway. A similar explanation was recently proposed to interpret the selective hydrogenation of cinnmaldehyde to cinnamyl alcohol on ternary Cu–Zn–Al catalysts [33].

Similarly to Cu–ZnO/SiO_2 sample, the high-temperature reduction treatment drastically increased the r^0_{CrOH}/r^0_{BAL} ratio on ternary CuZnAl samples (Fig. 5e–h). For example, r^0_{CrOH}/r^0_{BAL} was 0.037 on sample CuAlZn-1 reduced at 300 °C but increased to 0.270 after reducing the sample at 480 °C (Table 5). As in the case of Cu–ZnO/SiO_2, a high reduction treatment is required for promoting the formation of Cu^0–ZnO_x species, which favor the hydrogenation of the C=O bond of crotonaldehyde. However, we noted that the reduction temperature needed to drastically increase the initial CrOH selectivity is lower on ternary CuZnAl samples than on Cu–ZnO/SiO_2. Specifically, the required reduction temperature was 500 °C for Cu–ZnO/SiO_2, and 480 and 440 °C for CuAlZn-1 and CuAlZn-2 samples, respectively. This result may be explained by considering that Cu–ZnO/SiO_2 contains large copper crystallites (around 55 nm) while on ternary CuZnAl samples copper is well dispersed, forming metallic crystallites of about 2 nm. Thus, the Cu^0–ZnO_x interaction is expected to be more difficult to reach on Cu–ZnO/SiO_2, which thereby requires a higher reduction temperature to increase further the mobility of ZnO_x species. On the other hand, the fact that the reduction temperature needed to improve the CrOH selectivity is lower on CuAlZn-2 than on CuAlZn-1 would be related to the Zn content. In fact, CuZnAl-1 was prepared with a molar ratio Zn/Al = 1/2 which corresponds to the stoichiometric composition of $ZnAl_2O_4$ spinel phase. It is expected, therefore, that CuZnAl-1 show small amounts of ZnO extra to $ZnAl_2O_4$ structure available for the Cu^0–ZnO interaction. In contrast, Zn/Al molar ratio was 3/2 in CuZnAl-2 giving as stoichiometric formula $CuOZnO[ZnAl_2O_4]_2$ that contains ZnO extra to the structure of $ZnAl_2O_4$. Such an increase in the surface concentration of "free" ZnO_x species explains that lower reduction temperature is required to form Cu^0–ZnO_x species on CuZnAl-2 sample.

3.3.2. Catalyst activity and selectivity evolution on stream

Initially, crotonaldehyde conversion rate disminished with time on stream (Fig. 5 and Table 5) because of formation of carbonaceous residues on the catalytic surface. We observed that after about 60 min on stream the carbon balance was close to 100%, thereby suggesting that coke formation occurs essentially during the first hour of the catalytic run. In order to confirm these observations, we characterized samples by TPO technique after the deactivation period (i.e. after about 1 h on stream) and after 19 h on stream (i.e. at the end of the catalytic runs, the reaction under steady-state conditions). Results are given in Fig. 6. TPO profiles of Fig. 6 show that for all the samples the amount of coke determined after the initial deactivation period was practically the same than that measured after 19 h on stream,

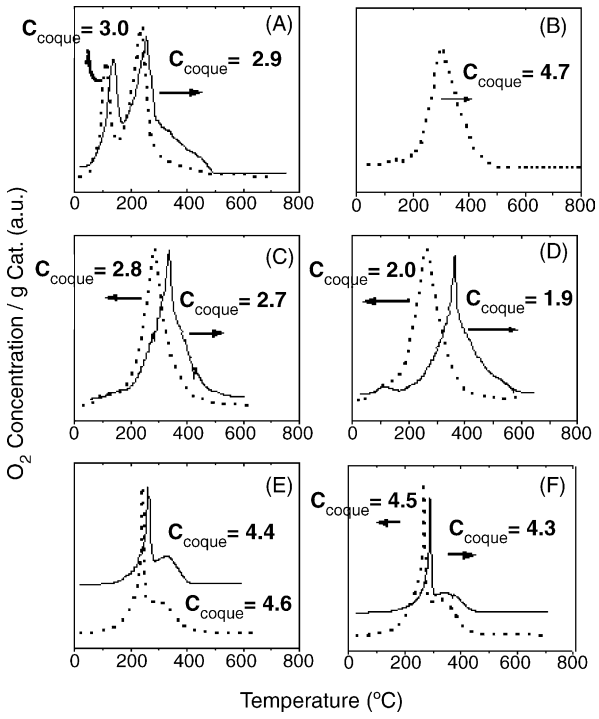

Fig. 6. TPO profiles of samples: (A) CuSi-LT, (B) CuAl-LT, (C) CuZnSi-LT, (D) CuZnSi-HT, (E) CuZnAl-2-LT, (F) CuZnAl-2-HT: . . ., after initial deactivation period; —, after 19 h of reaction.

thereby confirming that coke is essentially formed at the beginning of the reaction. As suggested by Coloma et al. [49], coke formation probably occurs via aldol condensation, dimerisation or condensation reactions when crotonaldehyde and hydrogen are feeding to the reactor. Our TPO characterization showed that the burnt of coke precursors on Cu–ZnO/SiO_2 reduced either at 300 or 500 °C gives rise to a wide O_2 consumption peak between 200 and 400 °C (Fig. 6c and d). The TPO profile of Cu/SiO_2 sample showed an additional low-temperature peak at about 150 °C arising probably from the combustion of reaction products adsorbed on the catalyst surface. Finally, ternary CuZnAl-2 sample reduced at 300 and 440 °C displayed sharp combustion peaks with maxima at 260 and 290 °C, respectively, which can be assigned to the presence of small metal particles dispersed in a nonstoichiometric spinel-type matrix.

In Table 5, we have included the product formation rates obtained at the end of the coke formation period (r_i^1 μmol g Cu^{-1} s^{-1}) and after 19 h on stream (r_i^2 μmol g Cu^{-1} s^{-1}). Once coke formation is completed on the catalyst surface, the qualitative changes of activity and selectivity with time on stream greatly depended on the catalyst tested. For example, product formation rates on Cu/SiO_2 and coprecipitated Cu–Al_2O_3 samples gradually felt after the initial deactivation period, reaching steady-states values at about 7 h on stream (Fig. 5a and b). Similar catalytic behavior was observed for ternary CuZnAl samples reduced at 300 °C (Fig. 5e and g). In contrast, on sample Cu–ZnO/SiO_2 reduced at 500 °C the butyraldehyde formation rate increased after the initial deactivation period reaching steady-state values at about 10 h on stream (Fig. 5d, CuZnSi-HT sample). Specifically, the r_{BAL} increased from 0.59(r_{BAL}^1) to 3.67(r_{BAL}^2) μmol g Cu^{-1} s^{-1} (Table 6), and as a consequence r_{CrOH}/r_{BAL} ratio diminished continuously with time on stream reaching finally a stable value of about 0.06 which is similar to that determined for Cu/SiO_2 after 19 h on stream.

In order to obtain insight on the r_{BAL} increase on stream for CuZnSi-HT sample (Fig. 5d), we performed an additional catalytic test. Specifically, fresh CuZnSi-HT was treated for 10 h under a N_2 flow at the reaction temperature (120 °C) before testing it for the standard crotonaldehyde conversion reaction. Initial catalyst activity and selectivity were similar to those determined when CuZnSi-HT was tested immediately after reduction at 500 °C (Table 6), thereby showing that pretreatment in N_2 at 120 °C did not modify the catalytic properties of sample CuZnSi-HT. In contrast, we observed that treating CuZnSi-HT with N_2O at 30 °C for 12 h significantly increases the metallic Cu area (Table 3), which indicated that this treatment partially destroys the Cu–ZnO_x interaction and liberates metallic copper. Similarly, we can expect that the r_{BAL} increase on stream observed in Fig. 5d for sample CuZnSi-HT reflects the gradual formation of metallic Cu sites very active for C=C hydrogenation from decomposition of Cu–ZnO_x species due to the presence of adsorbed oxygenate reactants and products on the catalyst surface. Thus, when decomposition of Cu–ZnO_x species is achieved, catalyst reaches steady-state conditions producing essentially butyraldehyde. In summary, our XRD, XPS, and catalytic results suggest that the high-temperature hydrogen treatment of sample Cu–ZnO/SiO_2 forms Cu^0–ZnO_x particles which promote the C=O hydrogenation of crotonaldehyde to crotyl alcohol, thereby changing the intrinsic selectivity of metallic Cu to the preferential formation of butyraldehyde. But the Cu^0–ZnO_x particles are unstable on stream and are progressively decomposed forming metal Cu particles, which concomitantly favor the selective C=C bond hydrogenation of crotonaldehyde.

Qualitatively, the selectivity changes after the initial deactivation period on ternary CuZnAl samples reduced at high temperatures were similar to those observed for CuZnSi-HT, i.e. r_{BAL} increased while the r_{CrOH}/r_{BAL} ratio decreased with time on stream (Fig. 5f and h). But the intensity of selectivity changes for CuZnAl samples depended on Zn/Al molar ratio. In fact, at the end of the initial deactivation period, CuZnAl-1-HT showed a r_{CrOH}^1/r_{BAL}^1 ratio of 0.44 (Table 5), which decreased to 0.12 when steady-state conditions were reached at about 300 min on stream. CuZnAl-2-HT showed a similar r_{CrOH}^1/r_{BAL}^1 ratio than CuZnAl-1-HT, but it decreased to only 0.24 after 19 h on stream. The lower decline rate of r_{CrOH}/r_{BAL} ratio on CuZnAl-2-HT as compared to CuZnAl-1-HT may be kinetically explained by considering that the concentration of surface Cu–ZnO_x species should be higher on CuZnAl-2-HT because it contains more ZnO. But

Cu–ZnO_x species formed on CuZnAl-2-HT are also probably more stable than on CuZnAl-1-HT. This difference in stability may arise from different Cu morphologies, as suggested by our FT-IR of adsorbed CO and the literature [50]. A different Cu morphology would result in a different interaction and mobility of ZnO when Cu–ZnO_x species are decomposed on stream to ZnO and Cu^0 on the catalyst surface.

4. Conclusions

The activity, selectivity, and stability for the gas-phase hydrogenation of crotonaldehyde on Cu–based catalysts greatly depend on both the catalyst composition and the reduction temperature. Impregnated Cu/SiO_2 and coprecipitated Cu–Al catalysts hydrogenate preferentially the C=C bond of crotonaldehyde on metallic copper and form initially more than 90% of butyraldehyde, irrespective of the reduction temperature. The initial product selectivities on impregnated Cu–ZnO/SiO_2 catalyst reduced at 300 °C are similar to that observed on Cu/SiO_2, but the formation rate of crotyl alcohol on Cu–ZnO/SiO_2 drastically increases when the sample is reduced at 500 °C. This enhancement of the C=O hydrogenation rate on Cu–ZnO/SiO_2 catalyst reduced at 500 °C is interpreted by considering that the high-temperature hydrogen treatment forms mobile reduced ZnO_x species that closely interact with Cu^0 crystallites and provide a new reaction pathway for selectively hydrogenating crotonaldehyde to crotyl alcohol. Specifically, crotonaldehyde would interact via the C=O bond with cationic Zn sites thereby favoring its selective hydrogenation to the unsaturated alcohol by atomic hydrogen activated on neighboring Cu^0 sites. The C=O hydrogenation rate is also drastically enhanced on Cu_x–Zn_yO_{2y}–$ZnAl_2O_4$ catalysts by high-temperature reduction, but the reduction temperature required to form Cu^0–ZnO_x active sites is lower than on Cu–ZnO/SiO_2 because small Cu^0 crystallites are well dispersed in the non-stoichiometric Zn_yO_{2y}–$ZnAl_2O_4$ spinel-like phase favoring its interaction with cationic Zn sites.

Dual Cu^0–ZnO_x surface sites on both Cu–ZnO/SiO_2 and Cu–Zn–Al catalysts are unstable during crotonaldehyde hydrogenation, probably because they are decomposed to Cu^0 and ZnO by the presence of adsorbed oxygenate products. Decomposition of Cu^0–ZnO_x species to metallic copper causes the continuous increase of the butyraldehyde selectivity on stream until steady-conditions are reached. The butyraldehyde formation increase on stream is markedly slower on Cu–Zn–Al than on Cu–ZnO/SiO_2 reflecting the higher stability of Cu^0–ZnO_x species in ternary Cu–Zn–Al catalysts.

Acknowledgments

We thank the financial support of FAPESP (Fundação para o Amparo a Pesquisa do Estado de São Paulo, Brazil), CNPq (Conselho Nacional de Desenvolvimento Cientifico e Tecnológico, Brazil), CONICET (Consejo Nacional de Investigaciones Cientificas y Técnicas, Argentina), and U.N.L. (Universidad Nacional del Litoral, Argentina). We are grateful to Dr. C. Querini for TPO measurements.

References

[1] M.A. Vannice, B. Sen, J. Catal. 115 (1989) 65.
[2] M.A. Vannice, J. Mol. Catal. 59 (1990) 165.
[3] V. Ponec, Appl. Catal. A 149 (1997) 27.
[4] F. Delbecq, P. Sautet, J. Catal. 152 (1995) 217.
[5] P. Beccat, J.C. Bertolini, J. Massardier, P. Ruiz, J. Catal. 126 (1990) 451.
[6] M. Englisch, A. Jentys, J.A. Lercher, J. Catal. 166 (1997) 25.
[7] H. Yoshitake, Y. Iwasawa, J. Catal. 125 (1990) 227.
[8] J. Kaspar, M. Graziani, G.P. Escobar, A. Trovarelli, J. Mol. Catal. 72 (1992) 243.
[9] P. Gallezot, A. Giroir-Fendler, D. Richard, Catal. Lett. 5 (1990) 169.
[10] D.G. Blackmond, R. Oukaci, B. Blanc, P. Gallezot, J. Catal. 131 (1991) 401.
[11] S. Galvagno, Z. Poltarzewski, A. Donato, G. Neri, R. Pietropaolo, J. Mol. Catal. 35 (1986) 365.
[12] F. Coloma, A.S. Escribano, J.L.G. Fierro, F.R. Reinoso, Appl. Catal. A 136 (1996) 231.
[13] G. Neri, L. Mercadante, C. Milone, R. Pietropaolo, S. Galvagno, J. Mol. Catal. A 108 (1996) 41.
[14] B. Bachiller-Baeza, I. Rodríguez-Ramos, A. Guerrero-Ruiz, Appl. Catal. A 205 (2001) 227.
[15] M. del, C. Aguirrea, P. Reyes, M. Oportusa, I. Melián-Cabrerab, J.L.G. Fierro, Appl. Catal. A 233 (2002) 183.
[16] G. Lafaye, T. Ekou, C. Micheaud-Especel, C. Montassier, P. Marecot, Appl. Catal. A 257 (2004) 107.
[17] M. Englisch, S. Ranade, J.A. Lercher, J. Mol. Catal. A: Chem. 121 (1997) 69.
[18] M. Abid, G. Ehret, R. Touroude, Appl. Catal. 217 (2001) 219.
[19] S. Galvagno, A. Donato, G. Neri, R. Pietropaolo, G. Capannelli, J. Mol. Catal. 78 (1993) 227.
[20] P. Kluson, L. Cerveny, Appl. Catal. A 128 (1995) 13.
[21] J.P. Candy, B. Didillon, E.L. Smith, T.B. Shay, J.M. Basett, J. Mol. Catal. 86 (1994) 179.
[22] S. Galvagno, Z. Poltarzewski, A. Donato, G. Neri, R. Pietropaolo, J. Chem. Soc., Chem. Commun. (1986) 1729.
[23] A.N. Patil, M.A. Bañares, X. Lei, T.P. Fehlner, E.E. Wolf, J. Catal. 159 (1996) 458.
[24] E.L. Rodrigues, C.E.C. Rodrigues, A.J. Marchi, C.R. Apesteguia, J.M.C. Bueno, in: A. Corma, F.V. Melo, S. Mendioroz, J.L.G. Fierro (Eds.), Advances in Chemical Conversions for Mitigating Carbon dioxide, vol. 130, Elsevier, Amsterdam, 2000, p. 2087.
[25] E.L. Rodrigues, J.M.C. Bueno, Appl. Catal. 232 (2002) 147.
[26] E.L. Rodrigues, J.M.C. Bueno, Appl. Catal. 257 (2004) 201.
[27] H. Noller, W.M. Lin, J. Catal. 85 (1984) 25.
[28] T.R. Bonelle, R. Hubant, M. Daage, Appl. Catal. 22 (1986) 231.
[29] A. Dandekar, R.T.K. Baker, M.A. Vannice, J. Catal. 184 (1999) 421.
[30] G.J. Hutchings, F. King, I.P. Okoye, M.B. Padley, C.H. Rochester, J. Catal. 148 (1994) 453.
[31] G.J. Hutchings, F. King, I.P. Okoye, C.H. Rochester, Catal. Lett. 23 (1994) 127.
[32] E.L. Rodrigues, A.J. Marchi, C.R. Apesteguia, J.M.C. Bueno, in: Proceedings of the 16th Meeting of the North American Catalysis Society, Boston, EUA, 1999, PI-009.
[33] A.J. Marchi, D.A. Gordo, A. Trasarti, C.R. Apesteguía, Appl. Catal. A: General 249 (2003) 53.
[34] F. Ammari, J. Lamotte, R. Touroude, J. Catal. 221 (2004) 32.

[35] M.J.L. Ginés, A.J. Marchi, C.R. Apesteguia, Appl. Catal. 154 (1997) 155.
[36] A.J. Marchi, J.L. Di Cosimo, C.R. Apesteguia, New frontiers in catalysis, in: L. Guczi, F. Solymosi, P. Tetenyi (Eds.), Proceedings of the 10th International Congress on Catalysis, vol B, Elsevier, Amsterdam, 1993, p. 1771.
[37] C.J.G. van Der Grift, A.F.H. Wielers, B.P.J. Joghi, J. van Beijnum, M. Boer, M. Versluijs-Helder, J.W. Geus, J. Catal. 131 (1991) 178.
[38] H. Berndt, V. Briehn, S. Evert, J. Mol. Catal. 73 (1992) 203.
[39] Th.J. Osinga, B.G. Linsen, W.P. van Beet, J. Catal. 7 (1967) 277.
[40] S.C. Fung, C.A. Querini, J. Catal. 138 (1992) 240.
[41] G. Fierro, M. Lo Jacono, M. Inversi, P. Porta, F. Cioci, R. Lavecchia, Appl. Catal. A 137 (1996) 327.
[42] T. Van Herwijnen, W.A. de Jong, J. Catal. 34 (1974) 209.
[43] J. Nakamura, T. Uchijima, Y. Kanai, T. Fujitani, Catal. Today 28 (1996) 223.
[44] J. Nakamura, I. Nakamura, T. Uchijima, Y. Kanai, T. Watanabe, M. Saito, T. Fujitani, J. Catal. 160 (1996) 65.
[45] E.K. Poels, D.S. Brands, Appl. Catal. A 191 (2000) 83.
[46] A. Dandekar, M.A. Vannice, J. Catal. 178 (1998) 621.
[47] M.A. Kohler, N.W. Cant, M.S. Wainwright, D.L. Trimm, J. Catal. 117 (1989) 188.
[48] H.S. Bengaard, J.K. Nørskov, J. Sehested, B.S. Clausen, L.P. Nielsen, A.M. Molenbroek, J.R. Rostrup-Nielsen, J. Catal. 209 (2002) 365.
[49] F. Coloma, J. Llorca, N. Homs, P.R. Piscina, F.R. Reinoso, A.S. Escribano, Phys. Chem. Chem. Phys. 2 (2000) 3063.
[50] B.H. Sakakini, J. Tabatabaei, M.J. Watson, K.C. Waugh, J. Mol. Catal. 162 (2000) 297.